Spiral Defect Formation in Friction Welded Aluminum

Spiral Defect Formation and the Factors Affecting the Mechanical Properties of Friction Welded Aluminum Were Investigated

BY K. UENISHI, Y. ZHAI, T. H. NORTH AND G. J. BENDZSAK

ABSTRACT. Spiral defect formation and the factors affecting the mechanical properties of friction welded aluminum Alloy 6061 T6 and 6061/Al_2O_3 (W6A.10A-T6) composite base materials were investigated. Spiral defects are flow-induced defects formed when material and reinforcing particles transfer to and are trapped in spiral arm regions located near the stationary boundary of friction welded joints. In MMC/MMC joints the spiral defects are Mg-rich and are associated with the segregation of small-diameter Al_2O_3 particles.

When high pressure is applied during 6061/6061 friction welding, the tensile strength properties are improved because of the formation of narrower softened regions on either side of the joint interface. The ratio of the width of the softened region and the tensile-specimen diameter are used to monitor the effect of softened regions on weld tensile-strength properties. Using this approach, the calculated and experimentally measured joint tensile-strength properties of 6061/6061 joints are in excellent agreement.

The improved strengths of MMC/MMC joints produced using high friction pressures resulted from a combination of factors, namely, 1) decreased numbers of spiral defects in completed joints, 2) material strengthening caused by increased numbers of reinforcing particles in material close to the weld interface and 3) the formation of narrower softened zones adjacent to the weld interface. The tensile strengths of MMC/MMC joints produced using a low friction pressure (60 MPa) were not improved following the application of a T6 solution plus aging postweld heat treatment. In direct contrast, the tensile strengths of postweld heat-treated MMC/MMC joints produced using a friction pressure of 280 MPa were significantly stronger than as-received MMC base material. It is suggested that the different effects produced during postweld heat treatment result from spiral defects acting as sites for preferential failure during notch tensile testing of joints made using low friction pressures.

K. UENISHI is Research Investigator, Department of Manufacturing Science, Osaka University, Osaka, Japan. Y. ZHAI is a Postdoctoral Fellow, T. H. NORTH is Professor and G. J. BENDZSAK is Associate Professor, Department of Metallurgy and Materials Science, University of Toronto, Toronto, Ontario, Canada.

Introduction

The high specific strength and specific stiffness properties of aluminum-based metal matrix composite materials compared with conventional aluminum base alloys readily explains why these materials are used in automotive and aerospace applications. At first glance, friction joining appears to be a natural candidate for joining aluminum-based composite material because of its brief joining period, minimal surface preparation before welding and ease of automation (Ref. 1). However, the high-temperature deformation cycle applied during the joining operation substantially alters the metallurgical and mechanical properties of material adjacent to the weld interface (Refs. 2–7). Also, particle fracture occurs when Al-based (Ref. 8) and Mg-based (Ref. 9) composite base materials are welded while particle agglomeration occurs in Fe-based MA956 friction welds (Ref. 10).

It has been reported the optimum notched tensile-strength properties are produced when high friction pressures are employed during friction welding of conventional aluminum alloys and aluminum-based composite materials (Refs. 11,12). Also, preferential failure during fatigue testing of MMC/MMC friction welds has been associated with spiral defect formation in completed joints (Ref. 11). However, convincing explanations for both effects have never been published.

This study presents the results of detailed experimental testing, transmission electron microscopy and numerical modeling. The influence of friction pressure on the microstructure and mechanical properties of 6061/6061 and MMC/MMC friction welds was investigated, and a detailed model for spiral defect formation is presented.

KEY WORDS

Aluminum
Composite Material
Friction Welding
Magnesium
Mechanical Properties
Postweld Heat Treatment
Spiral Defect Formation

Experimental Procedure

Aluminum alloy 6061-T6 and aluminum-based composite 6061/Al_2O_3 (W6A.10A-T6) materials were used throughout, in 19-mm-diameter bars. The metal matrix composite (MMC) base material had the nominal chemical composition of 0.28 wt-% Cu, 0.6 wt-% Si, 1 wt-% Mg, 0.2 wt-% Cr, balance aluminum and contained 10 vol-% Al_2O_3 particles, with an average particle size of 14 μm. The hardnesses of the as-received Alloy 6061 and MMC base materials were 120 and 70 HV, respectively.

Friction joining was performed using a direct-drive friction welding machine. The friction pressure was varied from 60 to 400 MPa while friction time, rotational

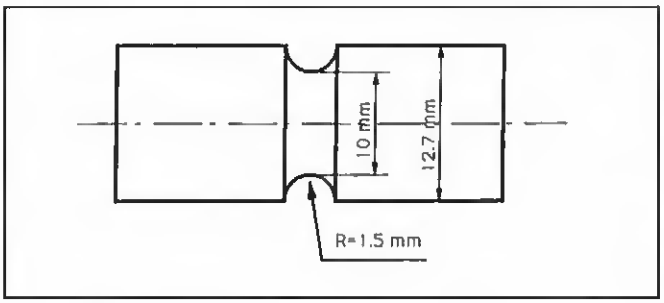

Fig. 1 — Design of the U-notch tensile specimen.

speed, forging pressure and forging time were maintained constant at 1 s, 1500 rpm, 240 MPa and 1 s, respectively.

It has been reported friction welding produces softened heat-affected-zone regions on either side of the weld interface and that postweld heat treatment satisfactorily counteracts this problem (Ref. 3). This aspect was examined in the present study via the application of two heat-treatment procedures, namely, 1) heat treatment involving solution treatment at 803 K for 2 h, followed by water quenching and then aging at 433 K for 16 h; and 2) heat treatment at 433 K for 16 h without a prior solution treatment of the test joint.

The microstructural features of completed joints were examined using a combination of optical, scanning electron (SEM) and transmission electron (TEM) microscopy. The test sections for TEM were thinned by electropolishing in a mixture of 6 vol-% perchloric acid and 94 vol-% methanol before ion milling using a voltage of 10 V at a temperature of 230 K.

The mechanical properties of all test joints were evaluated using a combination of hardness and U-notched tensile testing. Figure 1 shows the design of the notched tensile test specimens used in the present study. Duplicate testing was applied during mechanical testing. Spiral defects at the weld interface of completed joints could not be detected using conventional nondestructive examination techniques (ultrasonic testing and radiographic examination). For this reason, the defect frequency and the widths of defects produced during MMC/MMC and 6061/6061 welding were evaluated by point counting the defects observed on micrographs of notch tensile test specimen fracture surfaces.

Results and Discussion

Microstructural Features of 6061/6061 and MMC/MMC Joints

Figure 2 shows general views of 6061/6061 and MMC/MMC friction joints produced using different friction pressure values. It is convenient to describe the microstructural features of these joints using the nomenclature employed by Kang, *et al.* (Ref. 9), namely, the dynamically recovered microstructure at the weld interface is region RI, the upset region where the original base material grains are reoriented by the forging stage in friction joining is RII and the undeformed base material microstructure is region RIII — Fig. 3. Both dynamic recrystallization and dynamic recovery have been proposed as mechanisms for the microstructural evolution of material at the joint centerline (at the contact region) in rotary friction welds and in the plasticized region formed during friction stir welding. However, the most recent research indicates dynamic recovery is the most likely softening process in 6082-T6 and 7108-T79 friction stir welds.

Friction joining of aluminum alloy substrates combines high temperature with very high strain rates. For example, when AlSiMg (A357) alloy base material is friction welded, the tem-

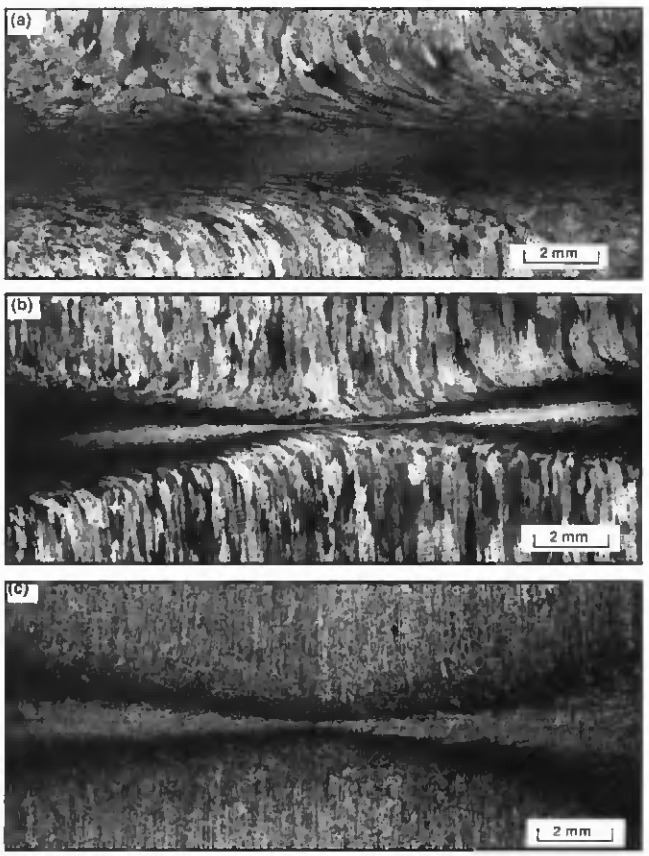

Fig. 2 — 6061/6061 and MMC/MMC weld profiles produced using different friction pressures: A — 6061/6061 joint produced using a friction pressure of 60 MPa; B — 6061/6061 joint produced using a friction pressure of 180 MPa; C — MMC/MMC joint produced using a friction pressure of 180 MPa.

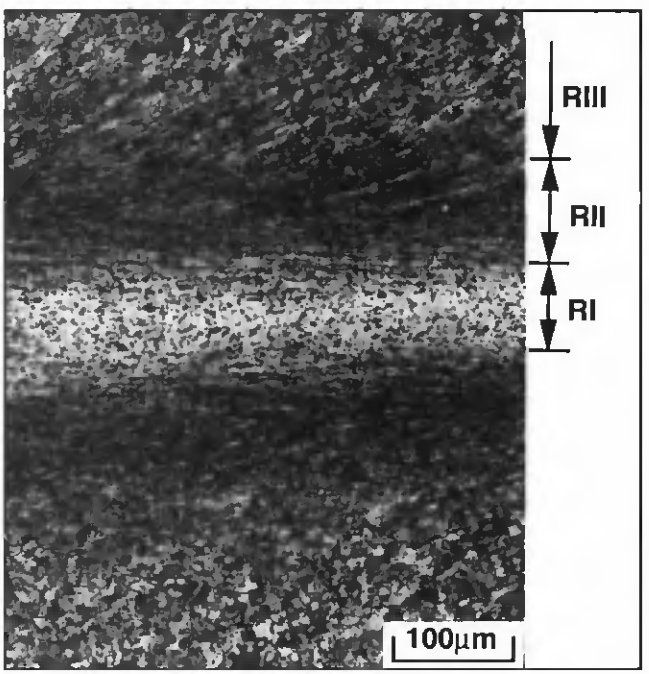

Fig. 3 — Regions RI and RII in friction welded joints. RI is the dynamically recovered region, RII is the region where base metal grains are oriented by the forging operation, and RIII is the as-received base material.

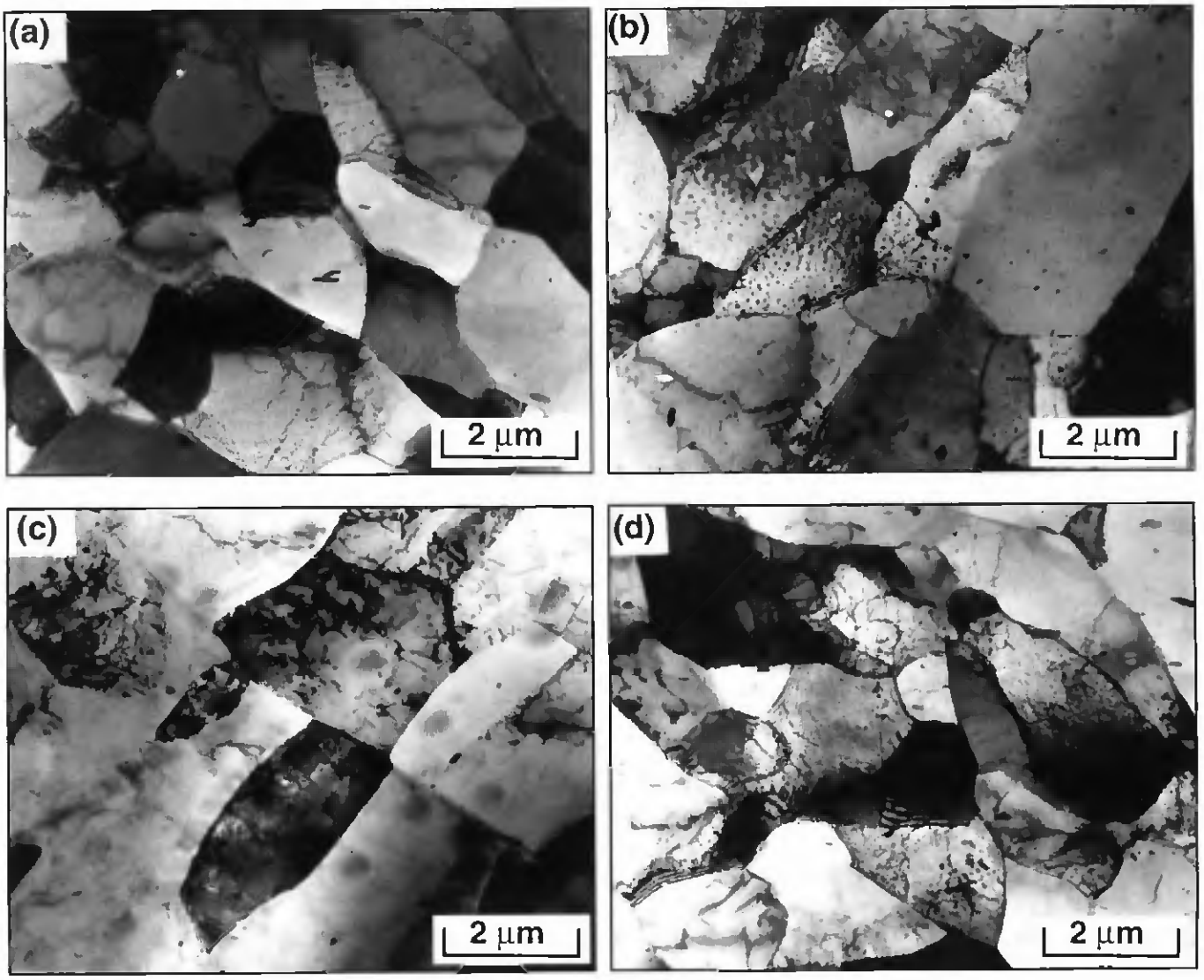

Fig. 4 — TEM micrographs showing the recrystallized region in 6061/6061 and MMC/MMC friction welded joints: A — At the periphery of a 6061/6061 joint; B — at the component centerline in a 6061/6061 joint; C — at the periphery of an MMC/MMC joint; D — at the centerline in an MMC/MMC joint.

Table 1 — Effect of Friction Welding Pressure on the Spiral Defect Frequency

Variable	Friction Pressure	
	30 MPa	120 MPa
Number of Spirals	34	3
Average Radial Spacing	150 μm	320 μm
Average Axial Spacing	15 μm	50 μm
Average Spiral Width	5 μm	13 μm
Minimum Radial Location	1800 μm	7100 μm
Maximum Width of Flow Zone	1100 μm	300 μm
Minimum Width of Flow Zone	120 μm	40 μm
Rotational Speed	1500 rpm	1500 rpm
Material	MMC/MMC 6061	MMC/MMC 6061

perature at the contact region is about 550°C and the calculated strain rate in the contact zone is as high as $10^4 s^{-1}$ (Ref. 3). This combination of high temperature and high strain rate deformation destroys the original base material microstructure at the contact region and replaces it with a fine-grained, dynamically recovered microstructure. Figure 4 shows TEM micrographs of the recovered regions produced in 6061/6061 and MMC/MMC friction welded joints. The equiaxed microstructure in the dynamically recovered region at the joint centerline is similar to that observed in hot-worked base materials. The subgrain dimensions (1–2 μm) were unchanged at increasing radial distance from the component centerline and when the friction pressure increased from 60 to 400 MPa.

During dynamic recovery, larger subgrain dimensions were formed when the temperature increased or the strain rate decreased. In contrast, finer subgrains were formed when the temperature decreased or the strain rate increased. During friction welding, higher strain rates occurred in regions away from the component centerline. Also, based on a first-order assumption that a constant pressure distribution and a constant effective frictional coefficient exist at the contact zone, it was expected that higher temperatures would be produced close to the joint periphery. However, the pressure distribution was not uniform for solid bars, so the effective coefficient of friction may not be constant at different locations across

the contact interface. Consequently, the assumption of higher temperatures at the joint periphery represented a major approximation. Fortunately, Zhai, *et al.* (Ref. 13), and Chernenko (Ref. 14) have produced experimental results confirming higher peak temperatures in material close to the joint periphery. As a result, it was suggested the negligible changes in subgrain dimensions at increasing radial distances from the component centerline resulted from the counteracting effects of higher strain rates and higher temperatures in such regions.

When fully plasticized material at the contact region was considered as a viscous fluid, the width of the fluid flow region as a function of radial location $h_{(r)}$ was determined by the relation (Ref. 15)

$$h_{(r)} = \eta \frac{2r^3\varpi}{\mu R_0^2 P_a} \qquad (1)$$

where η is the viscosity, r is the radius, ω is the rotational speed, μ is the coefficient of friction, R_0 is the outer radius and P_a is the applied pressure. Using Equation 1, the calculated flow width is very similar to that found in MMC/MMC friction welds (Ref. 15). Since heat generated by viscous dissipation at the contact region diffuses into the adjoining base materials, it would be expected the profiles of the dynamically recovered and softened zones would mirror that of the flow zone. Based on this argument, it would be expected the width of the fully plasticized region (R1) in MMC/MMC welds would be inversely proportional to the friction pressure applied during welding. This readily explains the experimental results shown in Fig. 5.

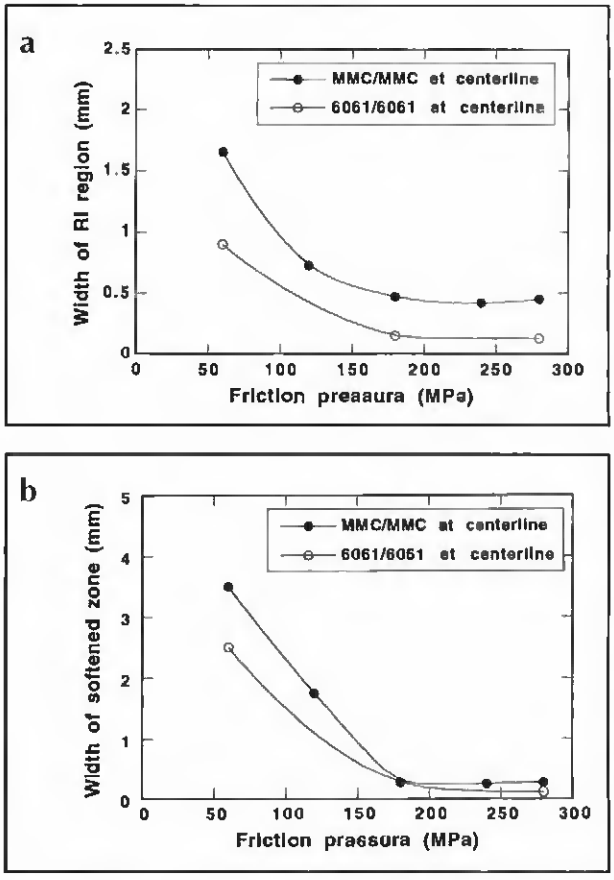

Fig. 5 — Effect of friction pressure on the widths of the RI region and the softened zone in 6061/6061 and MMC/MMC friction joints: A — Relation between friction pressure and RI; B — relation between friction pressure and the softened zone width.

Softened Zone Formation

Friction welding produced softened regions immediately adjacent to the weld interface (Fig. 6A), and postweld heat-treatment increased the hardness of the joint region to that of the as-received base material (Fig. 6B). Also, Fig. 6A shows the hardness variations in the radial direction at different axial distances from the joint centerline. Although there was a high dislocation density in material at the weld interface, there was no evidence of precipitation in the as-welded joint — Fig. 7A. In postweld heat-treated joints, however, the weld interface microstructure comprised fine needle-shaped β′ and β″ (Mg_2Si) precipitates, which had a preferred orientation parallel to the <100> direction in the α-aluminum matrix — Fig. 7B.

In as-welded joints, the widths of the softened regions on either side of the joint interface markedly decreased when higher friction pressures were applied — Fig. 5B. Based on Equation 1, it was expected the width of the softened zone formed during friction welding would be inversely proportional to the friction pressure applied during friction welding.

Spiral Defect Formation

Figure 8A shows spiral defect formation on the fracture surface of a notch tensile specimen machined from an MMC/MMC joint. The chemical composition of the spiral defect was markedly different from that of the surrounding material. In particular, the magnesium contents of spiral defects were much higher than that of the as-received 6061/Al_2O_3 base material — Fig. 8B. Also, the mag-

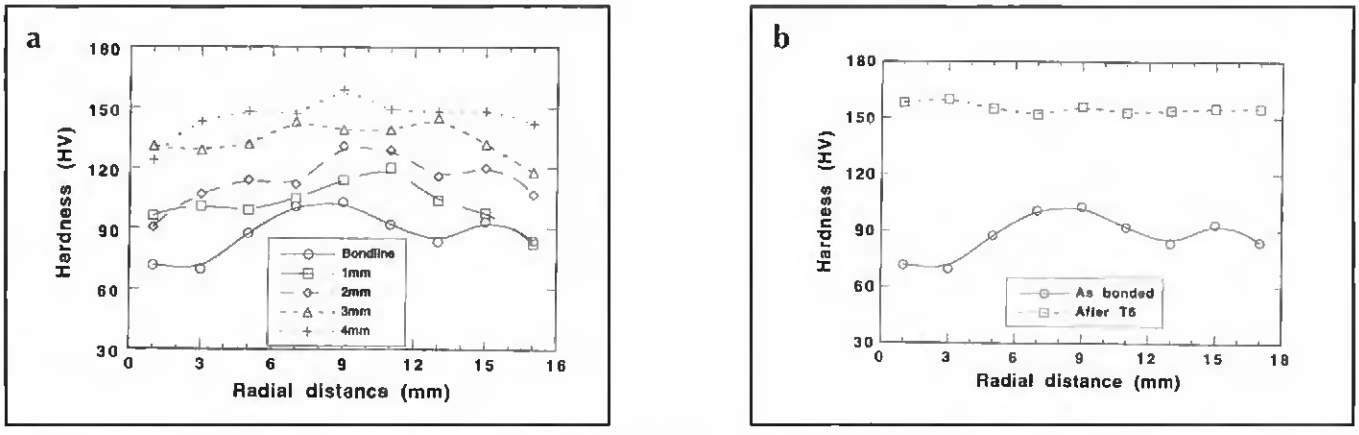

Fig. 6 — Hardness of 6061/6061 and MMC/MMC joints in the radial direction at different axial distances from the joint centerline: A — As-welded joints; B — joints given a T6 solution plus aging heat treatment.

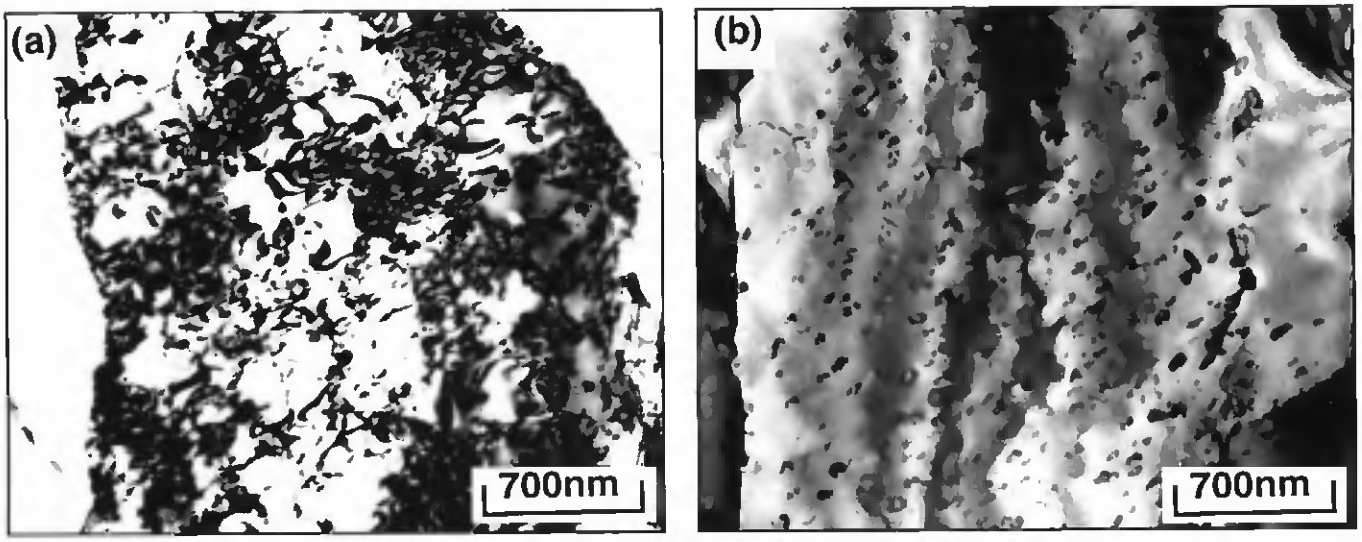

Fig. 7 — Subgrain structure in the dynamically recrystallized region R1 at the joint centerline of (A) an as-welded joint and (B) a solution-plus-aged joint.

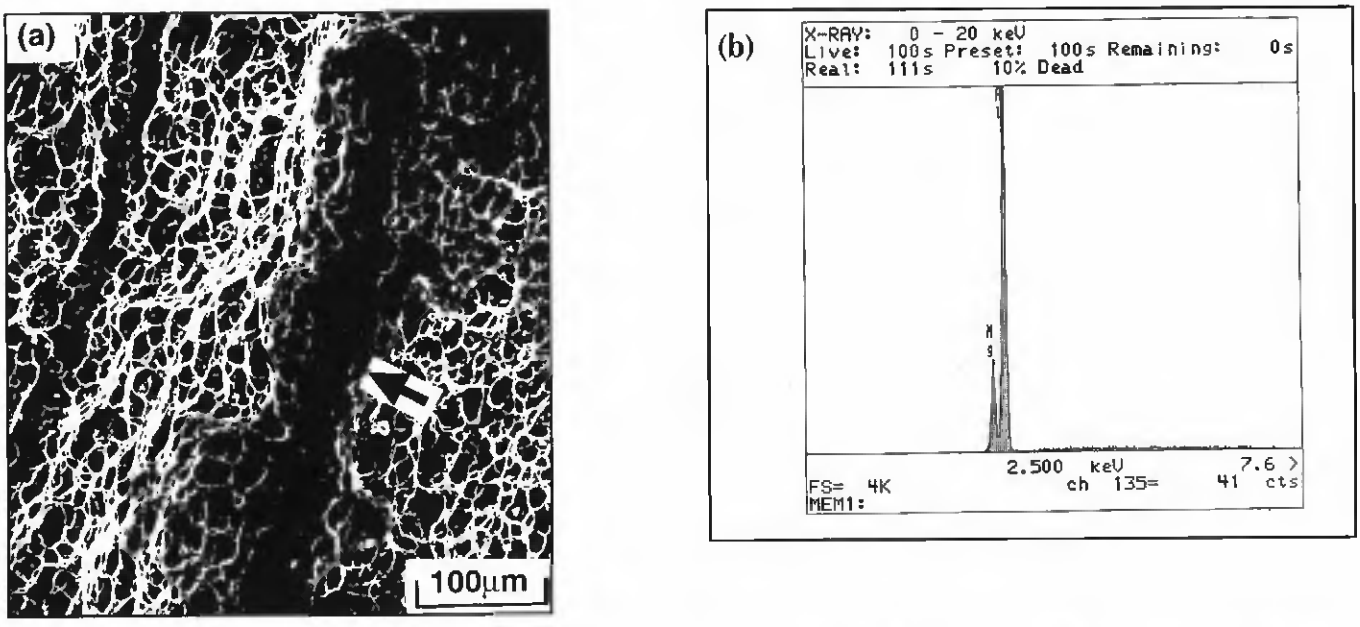

Fig. 8 — A — Spiral defects on the fracture surface of an MMC/MMC joint; B — EDX analysis of the spiral defect region showing high magnesium content.

nesium content varied considerably from one region to another along spiral defects. For example, some spiral defect regions contained as much as 55 wt-% Mg while others contained only 20 wt-% Mg. In some spiral defect areas, the high-magnesium-content regions were associated with localized solidification (hot) cracking — Fig. 9A. The spiral defects in MMC/MMC joints were also associated with the segregation of small (1- to 2-µm) diameter Al_2O_3 particles — Fig. 9B. Finally, the number and the widths of the spiral defects observed on the fracture surfaces of broken tensile-test sections markedly decreased when high friction pressures were applied during MMC/MMC welding — Fig. 10A, B.

Modeling of Spiral Defects

Fluid flow at the contact region has recently been numerically modeled during Al/Al friction welding by assuming solid material in this region acts as viscous fluid (Refs. 15–19). A detailed description of the numerical model has been published elsewhere, and, for this reason, only the basic features of the modeling approach are indicated here. A heuristic approach was adopted to estimate the parameters of a viscosity model, which accounted for shear thinning during the joining operation. (A heuristic approach is a trial-and-error methodology that substitutes values for unknown parameters, calculates the outcome and then repeats this process until a successful solution is attained.) The mechanical energy liberated in the weld zone was absorbed by viscous dissipation, and the viscosity relationships were approximated on the basis of negligible temperature gradients existing within the weld region. A steady-state, single-component, non-Newtonian flow regime was assumed between the stationary and rotating surfaces with radial growth occurring slowly and being represented by a series of stationary states.

The velocity boundary conditions at the rotating and stationary surface were derived based on an analysis of the flow of viscoplastic layers on either side of the flow zone. When it was assumed there

was a tangential variation in velocity along the line of demarcation between the flow region and the adjoining viscoplastic zones, material exchange across the boundaries did not occur but the momentum varied. Figure 11 shows the predicted flow patterns in Al/Al friction joints based on this assumption. These apply when Al/Al welding was performed using a friction pressure of 30 MPa, a friction time of 4.5 s and a rotational speed of 1500 rpm. The fluid flow pattern in Fig. 11 suggests the emergence of a series of spiral arms close to the stationary boundary of the welded joint in addition to transfer from the joint periphery toward the component centerline.

Although homogeneous aluminum, not particle-containing MMC base material, was considered in the numerical modeling, the Reynold's Number for the predicted flow is very low (<<1.00), and, therefore, creepy flow is being represented. Consequently, movement of reinforcing Al_2O_3 particles with the flow of plasticized material would he expected. There was excellent correspondence between the predicted and observed movement of Al_2O_3 particles in 6061/6061 joints where one substrate was capped with a 500-pm-thick MMC layer before welding (Ref. 18). In addition, particle movement closely conformed with the predicted fluid flow in 6061/6061 joints containing 1-mm-diameter MMC wire inserts at the component periphery (Ref. 18).

The results in Fig. 11 suggest spiral defects will form in both 6061/6061 and MMC/MMC joints. Figure 12A shows evidence of spiral defect formation in 6061/6061 joints and at the stationary boundaries of dissimilar MMC/AISI 304 stainless steel welds — Fig. 12B. Also, because of the characteristic shape of the friction welded joints, spiral defects formed at the stationary boundary were located at different distances from the joint centerline. This effect is schematically illustrated in Fig. 13. Finally, the calculated spiral arm frequency markedly decreased when the friction pressure increased (Table 1). These calculated results correspond well with the actual experimental results — Fig. 10.

Spiral arm regions are fluid-flow-induced discontinuities where material, agglomerations of magnesium-rich precipitates and reinforcing particles, is collected during the friction welding operation. With this in mind, these flow-induced defects should not have a uniform chemical composition, and the magnesium content should vary from one region to another along the defect length. In addition, Al_2O_3 particle segregation should be observed in spiral defects; this is confirmed in Fig. 8B. In this connection, it is suggested the localized hot cracking observed in some spiral defects results from liquation of Mg-rich material. The magnesium content of spiral defects ranged from 20 to 55 wt-% in MMC/MMC friction welds. A ternary eutectic alloy — having the approximate chemical composition of 35 wt-% Mg, <0.5 wt-% Si, remainder aluminum — solidifies at approximately 450°C in the Al-Mg_2Al_3-Mg_2Si system (Ref. 20). The localized hot cracks observed in some spiral defects may be associated with the formation of this eutectic alloy.

Notch Tensile Strength Properties

Figure 14 shows the influence of friction pressure on the notched tensile

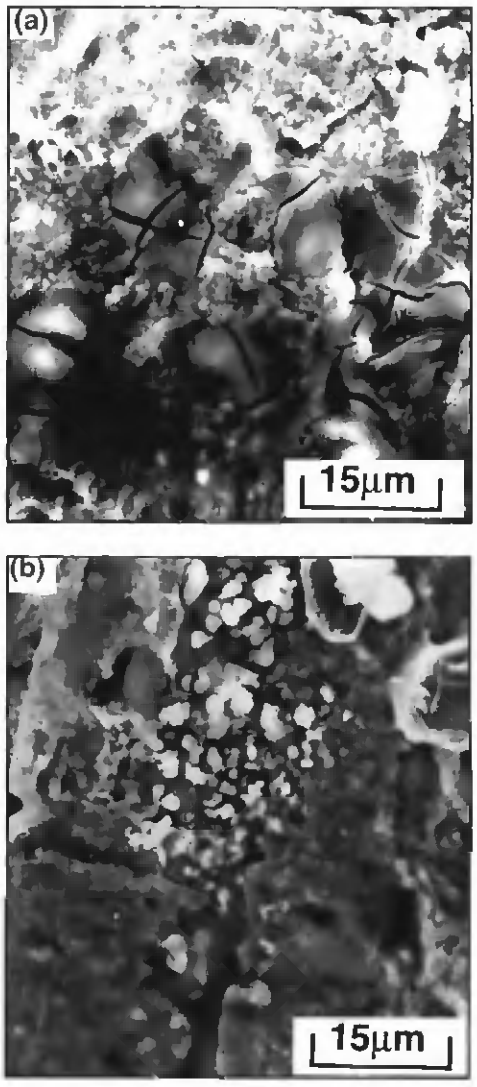

Fig. 9 — A — Localized hot cracks within a spiral defect; B — segregation of Al_2O_3 particles within a spiral defect.

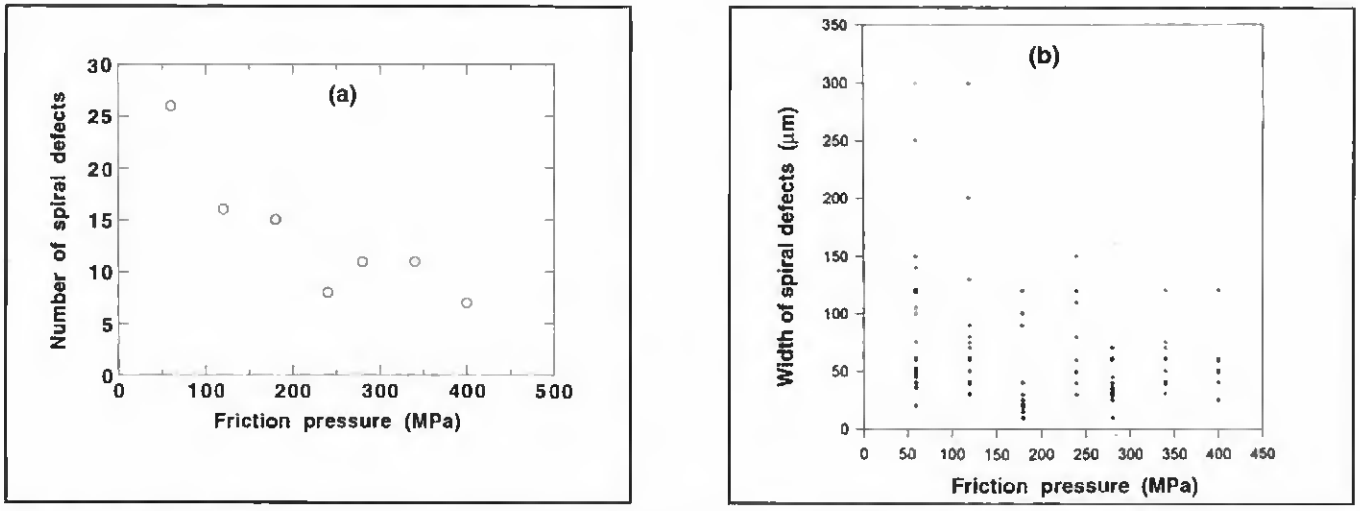

Fig. 10 — A — The influence of friction pressure on the spiral defect frequency in MMC/MMC friction welds; B — the influence of friction pressure on the width of spiral defects observed on the fracture surfaces of MMC/MMC friction joints (the points show the range of measured widths in joints produced using these friction pressures).

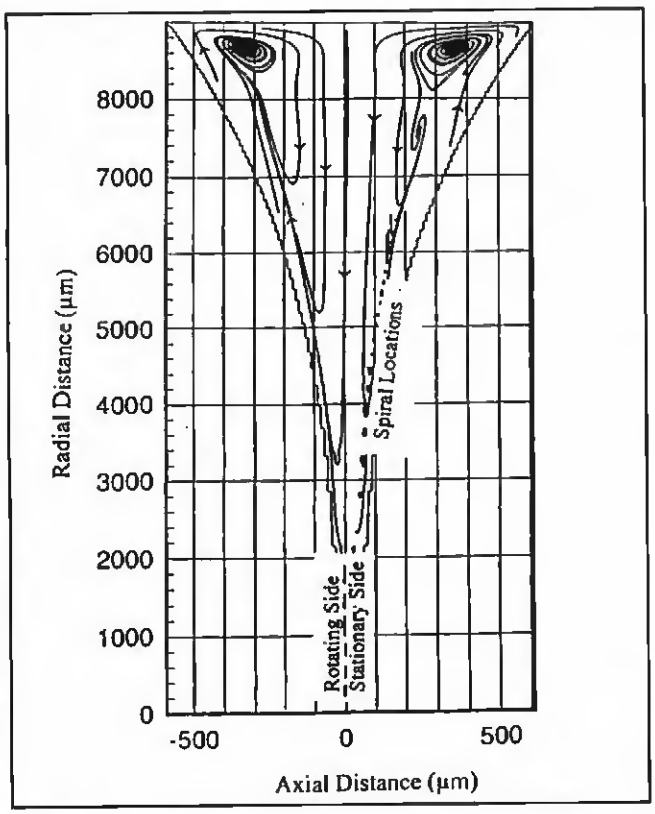

Fig. 11 — Predicted fluid flow patterns in an Al/Al joint when it is assumed there is a tangential variation in velocity along the line of demarcation between the flow region and the adjoining viscoplastic zones (for a friction pressure of 30 MPa, a friction time of 4.5 s, a forging pressure of 30 MPa and a rotational speed of 1500 rpm).

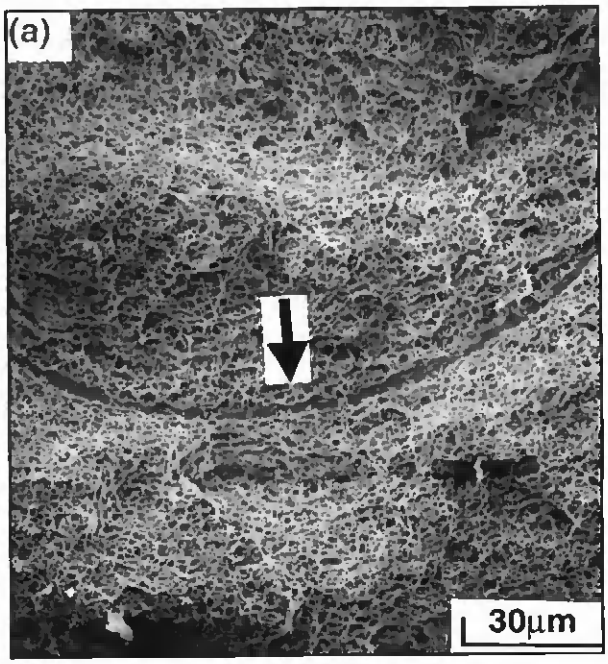

Fig. 12 — A — Spiral defects on the fracture surface of a 6061/6061 joint; B — spiral defects located at the stationary (MMC) boundary of a dissimilar MMC/AISI 304 stainless steel weld (the arrows show the locations of the spiral defects).

strengths of 6061/6061 and MMC/MMC friction joints. The notched tensile strength increased when high friction pressures were used during both 6061/6061 and MMC/MMC friction joining. However, the tensile strengths of the as-welded 6061/6061 and MMC/MMC joints were lower than the as-received base materials. The joint strength increased to 385 MPa, close to that of the as-received base material (400 MPa) when 6061/6061 welds were postweld heat-treated at 433 K for 16 h (without a prior solution treatment). Following a T6 solution plus aging heat treatment, the strength of 6061/6061 joints increased to 435 MPa and exceeded that of the as-received base material. The lower-strength properties of 6061/6061 joints heat treated at 433 K for 16 h without prior solution treatment can be explained by the further coarsening of over-aged Mg_2Si particles originally contained in the as-welded heat-affected-zone region.

Softened Region Formation and Joint Mechanical Properties

Satoh and Toyoda (Ref. 21) examined the effect of softened regions immediately adjacent to the joint interface on the ultimate tensile strength of constructional steel fusion welds. In their study, the parameter X_s (the ratio of the width of the softened zone region [H] and the tensile-specimen diameter [D]) was used to monitor the effect of softened regions on tensile strength properties. When X_s was very small, the tensile strength of steel fusion welds was similar to that of the as-received base material.

In the present study, the X_s value decreased from 0.6 to 0.2 when the friction pressure increased from 60 to 280 MPa during 6061/6061 friction welding.

For the notched tensile specimens design used in the present study (see Fig. 1), the relation between the nominal stress (σ_z) and the engineering strain (ε_z) in the necked region can be represented using the following equations:

$$\sigma_z = K\left[\ln\left(1+\varepsilon_z\right)\right]^n\left[\left(1+Y\right)\right]\left[\left(1+\frac{\varepsilon_z}{2}\right)\right]^2 \quad (2)$$

$$Xs = \frac{1}{2}\left[1-\frac{\varepsilon_z}{2}\right]^2\left[\sqrt{\frac{\varepsilon_z\left(1-\frac{\varepsilon_z}{2}\right)}{Y}-\varepsilon_z^2}\right]+$$

$$\frac{1}{6}Y\left[\sqrt{\frac{\varepsilon_z\left(1-\frac{\varepsilon_z}{2}\right)}{Y}-\varepsilon_z^2}\right]^3 \quad (3)$$

where n = the strain-hardening component of the material and Y = the numerical value produced using given values of X_s and σ_z.

Figure 15 shows the excellent correspondence between the calculated and experimentally measured notch tensile strengths of 6061/6061 friction joints containing different softened zone widths. In these calculations, the strain-hardening coefficient was 0.2. In a similar manner to Satoh and Toyoda's results (Ref. 21), the tensile strengths of 6061/6061 friction welded joints tended toward the ultimate tensile strength (400 MPa) of as-received Alloy 6061-T6 base material when X_s became very small.

Mechanical Properties of MMC/MMC Joints

The above argument partially explains the improved tensile strength of as-welded MMC/MMC joints produced using a high friction pressure. However, the situation is much more complex in MMC/MMC joints because 1) the particle size and interparticle spacing of reinforcing particles are altered by the friction joining operation and 2) spiral defects are formed at the weld interface of MMC/MMC joints — Fig. 10.

Particle Fracture during Friction Welding

Figure 16 compares the reinforcing Al_2O_3 particles observed in as-received 6061/Al_2O_3 (W6A.10A-T6) base material and in material immediately adjacent to the MMC/MMC joint interface. The MMC/MMC friction welding operation fragments reinforced Al_2O_3 particles in the as-received base material and produced an average particle radius of approximately 3 μm in material close to the weld interface. Maldonado and North (Ref. 22) reported that reinforcing Al_2O_3 particles in the MMC base material fractured very early in the joining operation and were retained at the weld interface because of fluid flow of fully plasticized material. The higher number of reinforcing particles in material adjacent to the joint interface in MMC/MMC welds increased the strength of material close to the joint interface — Fig. 16.

Preferential Failure at Spiral Defects

Following solution plus aging treatment, the tensile strength of MMC/MMC welds produced using a high friction pressure (280 MPa) increased to 500 MPa; this exceeded the tensile strength of the as-received base material (400 MPa). However, this postweld-heat-treatment cycle did not significantly improve the strength of MMC/MMC welds produced using a friction pressure of 60 MPa — Fig. 14.

Figure 17 shows a cross section through the fracture surface of the postweld-heat-treated MMC/MMC joint produced using a low friction pressure (60 MPa). It is suggested the strength of this joint is decreased as a result of spiral defects acting as sites for preferential failure. It has already been shown spiral defects are associated with hot cracks and segregation of small-diameter Al_2O_3 particles — Fig. 9A, B. It is suggested cracks and segregated alumina particles act as sites for preferential ductile failure during notch tensile testing. Based on this argument, the beneficial effect of postweld heat treatment in removing softened regions on either side of the MMC/MMC joint interface cannot counteract the detrimental influence of spiral defects on weld tensile-strength properties. Postweld heat treatment is most effective when MMC/MMC friction welds are produced using a high friction pressure. Following postweld heat treatment of MMC/MMC joints produced using a high friction pressure (280 MPa), the tensile strength exceeded that of as-received MMC base material because of 1) decreased numbers of spiral

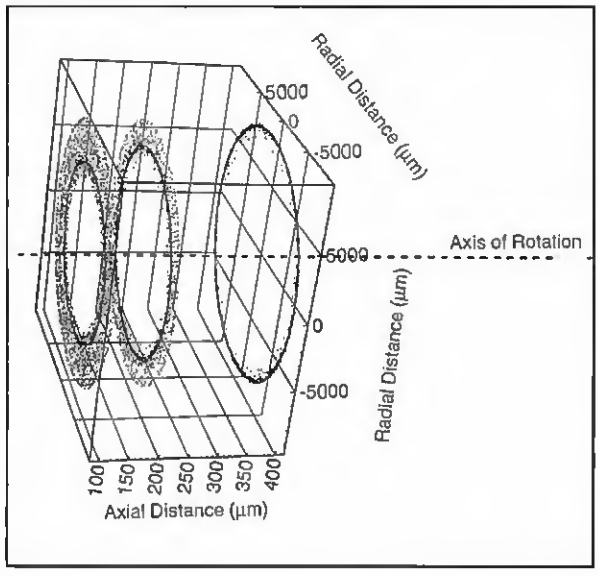

Fig. 13 — Schematic representation of spiral defect formation in regions located at different distances from the joint centerline.

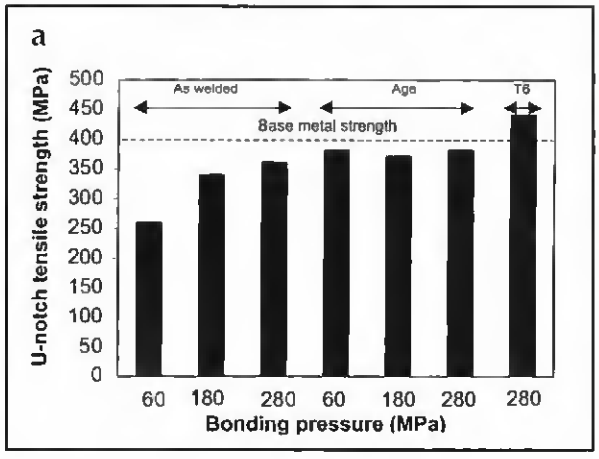

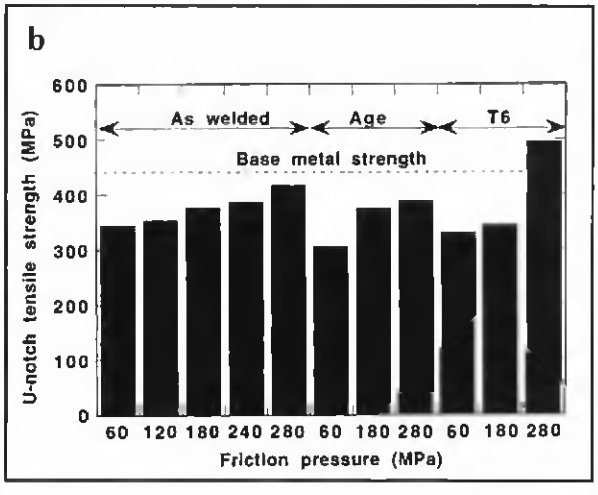

Fig. 14 — Effect of friction pressure on the notched tensile strength of (A) 6061/6061 and (B) MMC joints. In this figure, "Age" refers to the welded joints that have been aged but not solution treated before aging; T6 refers to welded joints that have been aged following solution treatment.

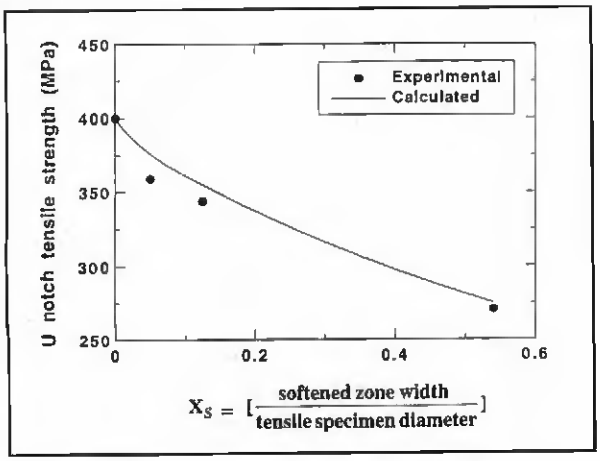

Fig. 15 — Calculated and experimentally measured notch tensile strengths of 6061/6061 joints.

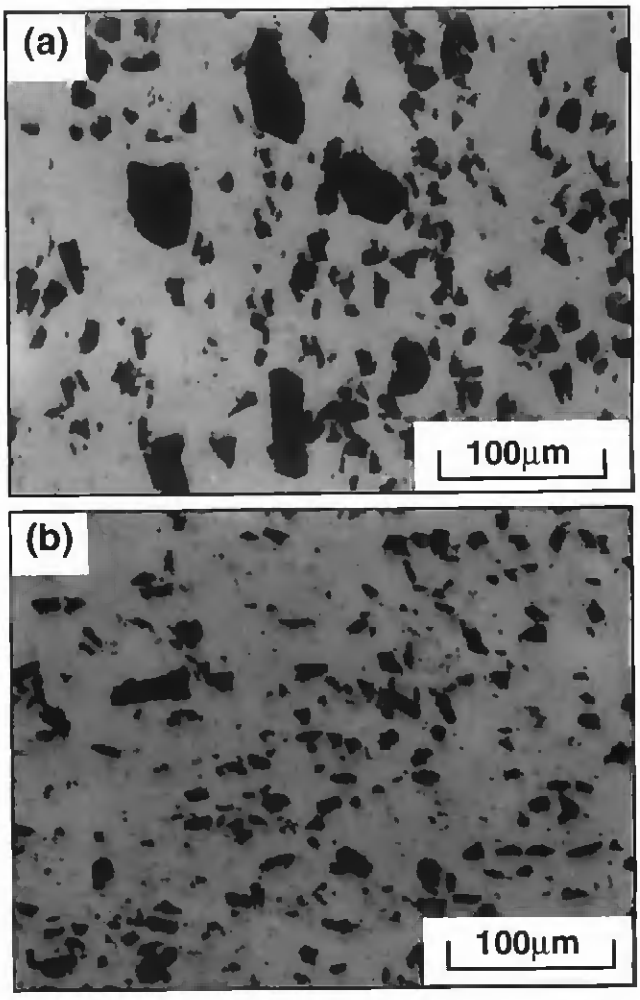

Fig. 16 — Al_2O_3 particles in (A) as-received MMC base material and (B) in material immediately adjacent to the MMC/MMC joint interface.

defects in completed welds and 2) small numbers of fragmented Al_2O_3 particles in material close to the weld interface.

Conclusion

Spiral defect formation and the factors determining the mechanical properties of 6061/6061 and MMC/MMC friction joints were examined in detail. A combination of experimental testing, TEM microscopy and numerical modeling has confirmed the following:

1) Spiral defects are fluid-flow-induced defects formed when material and reinforcing Al_2O_3 particles transfer to and are trapped in spiral arms located near the stationary boundary of friction welded joints. Spiral defects formed in MMC/MMC welds had high magnesium contents, contained localized hot cracks and were associated with Al_2O_3 particle segregation. It is suggested the regions containing localized hot cracks result from liquation of Mg-rich material within spiral defects. Finally, the application of high friction pressures during welding markedly decreased the incidence of spiral defects in MMC/MMC welds.

2) The improved notched tensile strength properties of 6061/6061 joints made using high friction pressures resulted from the formation of narrower softened regions immediately adjacent to the weld interface. The ratio of the width of the softened region (H) and the tensile specimen diameter (D) was used to monitor the influence of softened regions on weld tensile strength properties. Using this approach, the calculated and experimentally measured notch tensile strengths of 6061/6061 joints were in excellent agreement.

3) The improved tensile strengths of the MMC/MMC joints produced using high friction pressures resulted from a combination of factors, namely, decreased numbers of spiral defects in completed welds, material strengthening caused by larger numbers of fragmented alumina particles in material close to the weld interface and formation of narrower softened zones immediately adjacent to the joint interface.

4) The tensile strengths of MMC/MMC joints produced using a low friction pressure (60 MPa) were not improved by a T6 solution plus aging postweld heat treatment. In direct contrast, the tensile strengths of postweld-heat-treated MMC/MMC joints produced using a high friction pressure (280 MPa) were significantly stronger than the as-received MMC base material. It is suggested the lower tensile strengths of MMC/MMC joints produced using a low friction pressure (60 MPa) resulted from spiral defects acting as sites for preferential failure during mechanical testing.

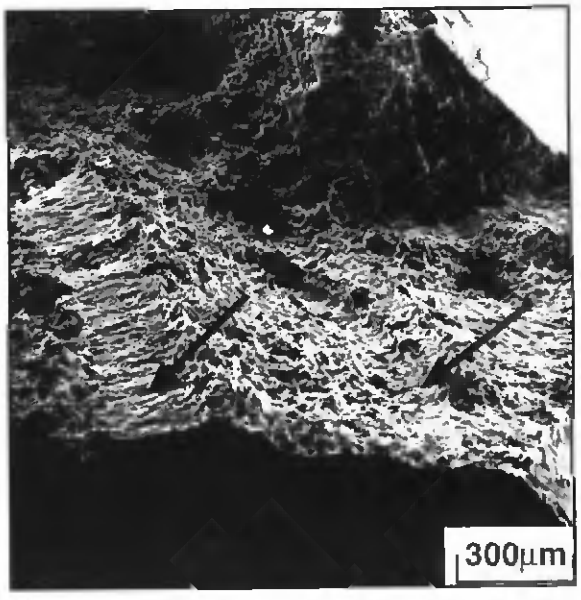

Fig. 17 — Fracture surface of a broken tensile test specimen machined from an MMC/MMC joint. The arrows show spiral defects on the fracture path.

Acknowledgments

The authors wish to acknowledge funding from the Ontario Center for Materials Research (OCMR). They would also like to thank

ALCAN International for supplying the aluminum-based MMC and for detailed technical assistance throughout this project.

References

1. Wang, K. K. 1975. Friction welding. *WRC Bulletin* 204, p. 1–21.

2. Midling, O. T., and Grong, O. 1994. A process model for friction welding of Al-Mg-Si alloys and Al-SiC metal matrix composites, Part 1: HAZ temperature and strain rate distribution. *Acta. Metall. and Mater.* 42(5): 1595–1609.

3. Midling, O. T., and Grong, O. 1991. A first report on the microstructural integrity and mechanical performance of friction welded Al-SiC composites. *Proc. of the 12th Riso Int. Symp. on Materials Science.* Riso International Laboratory, Denmark, pp. 529–534.

4. Cola, M. J., and Baeslack, W. A. 1993. Inertia friction welding of a particulate reinforced aluminum matrix composite. Third International SAMPE Conference, M424, 3. Toronto, Ontario, Canada.

5. Kreye, H., and Reiner, G. 1986. Metallurgical aspects and applications of friction welding. *Proc. ASM Conference: Trends in Welding Research.* Ed. S. A. David. ASM International, Materials Park, Ohio, pp. 307–310.

6. Kato, K., and Tokisue, H. 1995. Friction welding of magnesium alloys. *Japan Welding Institute* 9(5):352–356.

7. North, T. H. 1996. Friction joining of particle reinforced composites. *Proc. 6th Inter. Symp.: The Role of Welding Science and Technology in the 21st Century.* Ed. M. Ushio, Nagoya, pp. 673–682.

8. Zhou, Y., Li, Z., and North, T. H. 1995. Mechanical properties of particulate MMC/AISI 304 friction joints. *ISIJ International* 35(10): 1315–1321.

9. Ellis, M. B. D. 1994. Joining aluminum to steel, part 2 — friction welding. *Metal Construction,* pp. 171–175.

10. Kang, C. Y., North, T. H., and Perovic, D. D. 1996. Microstructural features of friction welded MA 956 superalloy material. *Metall.Trans.* 27A (12): 4019–4029.

11. Zhou, Y., Zhang, J., North, T. H., and Wang, Z. 1997. Mechanical properties of friction welded aluminum-based MMC material. *J. Mat. Sci.* 32: 3883–3889.

12. Li, Z. Maldonado, C., North, T.H., and Altshuller, 8. 1997. Mechanical and metallurgical properties of MMC friction welds. *Welding Journal* 76(9): 367-s to 373-s.

13. Zhai, Y., Maldonado, C., and North, T. H. 1998. Intermetallic formation and mechanical properties in dissimilar MMC/AISI 304 stainless steel friction welds. *J. Mater. Sci.* 33: 1–4.

14. Chernenko, I. A. 1989. Friction welding AD1 aluminum to 12KH18N10T steel. *Weld. Res. International* 7: 586–589.

15. Bendzack, G. J., North, T. H., and Li, Z. 1997. Numerical modeling of steady-state flow. *Acta Metall. Mater.* 45(4): 1735–1745.

16. Bendzsak, G. J., and North, T. H. 1996. Modelling of friction joining through the equations of fluid mechanics. *Proc. Sym., Prediction Theory of Welding and Joining,* Japan Joining and Welding Research Inst., Osaka, Japan, pp. 26–27.

17. Bendzack, G. J., and North, T. H. 1996. Trans. Modelling of viscosity and fluid dynamics in similar friction joints. *Jpn. Weld. Res. Inst.* 25(2): 171–184.

18. North, T. H., Bendzsak, G. J., Li, Z., and Zhai, Y. 1997. Particle retention and fluid flow in metal matrix composite friction welds. *Metall. Trans.* 28(11): 2371.

19. Bendzsak, G. J., and North, T. H. 1997. *Proc. International Seminar, Numerical Analysis of Weldability,* Graz, Austria.

20. *Metals Handbook, Vol. 8, Metallography, Structures and Phase Diagrams.* 1985. ASM International, Materials Park, Ohio.

21. Satoh, K., and Toyoda, M. 1975. Joint strength of heavy plates with lower strength weld metal. *Welding Journal* 54(9): 311-s to 318-s.

22. Maldonado, C., and North, T. H. 1997. Particle fracture in metal matrix composite friction joints. *J. Mat. Sci.* 32(3): 4739–4748.

FATIGUE OF BUTT-WELDED PIPE AND EFFECT OF TESTING METHODS

Report 1: Fatigue of Butt-Welded Pipe
by R. J. Scavuzzo, T. S. Srivatsan and P. C. Lam

Report 2: Effect of Testing Methods on Stress Intensification Factors
by E. C. Rodabaugh and R. J. Scavuzzo

Report No. 1 combines the results of two bending fatigue studies on butt-joint-welded pipe: one on 1 ½ in. Schedule 80 pipe and the other on 4-in. Schedule 40 pipe. The main objectives of these two investigations are to extend the fatigue database of butt-joint-welded pipe from Markl's tests into the low cycle range (100 to 2000) and to compare the measured fatigue strength with formulas developed by Markl of stress amplitude vs. cycles to failure. Secondary objectives are to investigate the effects of pipe size and field welds on the fatigue strength of butt-joint-welded pipe. Butt-joint-welded pipe specimens were tested using two different four-point bending test fixtures designed and fabricated for these test programs: fourteen1 ½-in. Schedule 80 A53 carbon steel specimens, seven 1 ½-in. Schedule 80, A312, Type 304 SS specimens, fifteen 4-in. Schedule 40 A106 carbon steel specimens, and three 4-in. Schedule 40 Type 304 SS specimens. All testing was conducted by prescribing constant cyclic alternating displacement amplitudes about a zero mean value. Force deflection data were taken so that results could be compared with Markl's stress data. Strain amplitudes were also measured so those strain-cycle curves could be developed for butt-joint-welded pipes.

Report No. 2 investigates the "difference" between cantilever testing and 4-point testing. A simple theory for elastic-plastic bending of pipe is developed and described. This theory does not represent any local discontinuity such as a girth butt-joint weld. Test data are described and theory is compared with the test data. The major uncertainty in these comparisons is the choice of Ep/E. Cantilever and four-point testing theoretically give the same results in the elastic regime. However, in the plastic regime, the theory indicates that there is a "difference" in the i-factors developed by different testing methods. The appropriateness of testing methods is discussed, leading to the opinion that, for elastic analysis of piping systems, cantilever testing is preferred because this method provides the most "elastic follow-up."

Publication of this document — **WRC Bulletin No. 433** — was sponsored by the Pressure Vessel Research Council of the Welding Research Council.

The price of **WRC Bulletin 433** (July 1998, 79 pages) is $90.00 per copy plus $5.00 for U.S. and Canada and $10.00 for overseas postage and handling. Orders should be sent with payment to the Welding Research Council, 3 Park Avenue, 27th Floor, New York, NY 10016-5902. Phone (212) 591-7956; Fax (212) 591-7183; E-mail wrc@forengineers.org or visit our home page *http://www.forengineers.org/wrc.*